ATMOSPHERIC TRANSMISSION IN THE REGION FROM 16.75 TO 20.95 MICROMETERS

by W. L. Raine
S. M. Landrum
M. W. Segewitz

July 1970

TELEDYNE
BROWN ENGINEERING

Research Park • Huntsville, Alabama 35807

TECHNICAL NOTE SE-300

ATMOSPHERIC TRANSMISSION IN THE REGION
FROM 16.75 TO 20.95 MICROMETERS

By

W. L. Raine
S. M. Landrum
M. W. Segewitz

July 1970
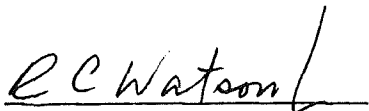
ABSTRACT

Preliminary solar spectrum observations covering the region from 16.75 to 20.95 micrometers under low resolution have been taken at a site on Bigelow Mountain, Arizona. These observations have been analyzed for the selective atmospheric transmission in the interval. From these data, transmission coefficients have been deduced which allow calculation of the selective transmission for various band model approximations. The fit of the observations to the various band model approximations has also been numerically evaluated throughout the region.

Approved:

R. C. Watson, Jr.
Vice President,
    Director of Research

TABLE OF CONTENTS

LIST OF ILLUSTRATIONS

LIST OF SYMBOLS

A_s Area of the entrance slit of the telescope-spectrometer

A_T Collecting area of the telescope optics

$B(\lambda, T)$ Planck radiation function expressed as a radiance

C_1 Attenuation coefficient for the strong-random band model approximation, air mass argument

C_2 Attenuation coefficient for the weak band model approximation, air mass argument

C_3 Attenuation coefficient for the strong-regular band model approximation, air mass argument

C_4 Attenuation coefficient for the strong-random band model approximation, precipitable water argument

C_5 Attenuation coefficient for the weak band model approximation, precipitable water argument

C_6 Attenuation coefficient for the strong-regular band model approximation, precipitable water argument

d Absorption line spacing for the Elsasser band model; the mean line spacing for the random model

F Focal length of the telescope

m Air mass

$P(S)\, dS$ Probability of occurrence of a spectral line of intensity between S and $S + dS$

$R_D(\lambda)$ Detector responsivity

S Intensity of a spectral line

S_0 Parametric mean line intensity occurring in the probability distribution of line intensities

u Amount of absorbing material (mass/unit area) in the line of sight

V	Signal voltage indicated by the telescope-spectrometer
V_0	Extraterrestrial signal voltage
w	Precipitable water in the path
X	Quantity $Su/(2\pi\alpha)$
X_0	Quantity $S_0 u/(2\pi\alpha)$
Z	Variable of integration
α	Half-width of an absorption line
β	Quantity $2\pi\alpha/d$
λ	Wavelength
$\Delta\lambda(\lambda)$	Spectral split width
τ	Transmission
$\tau_s(\lambda)$	Effective transmission of the telescope-spectrometer optical system, including mirror reflectivities, grating efficiency, and filter transmission
$\odot$	Subscript referring to solar measurements

INTRODUCTION

The transparency of the atmosphere in the infrared is of interest in a number fields, including infrared astronomy, geophysics, and atmospheric physics. Transmission data are needed by geophysicists to calculate the heat balance of the surface, and such data are useful to atmospheric physicists to study the absorptive and re-emissive properties of the atmosphere.

Selective transmission data are needed particularly by infrared astronomers for the correction of radiometric observations of celestial objects. Such radiometric observations are often made in bands several micrometers in width. Since the radiant spectral energy of astronomical sources and the atmospheric transmission are wavelength-dependent, any average transmission over a band will depend somewhat upon the radiant spectral energy distribution of the source. For sources which approximate black body emitters, such as the Moon, this spectral energy distribution is a function of a single parameter, i.e., the temperature. For such objects, the average transmission over the wavelength band being used, which is needed to correct the radiometric data, is therefore dependent upon the source temperature, which is the quantity sought. Selective atmospheric transmission data are both necessary and sufficient (Ref. 1) to correct for this dependence.

The atmospheric attenuation of infrared solar radiation passing through a clear sky is of the following two types:

- Continuum attenuation caused by scattering and absorption by particulate matter and aerosols suspended in the atmosphere, and the integrated absorption of the wings of the many distant absorption lines distributed throughout the spectrum

- Selective absorption by many thousands of absorption lines forming the absorption bands of the various molecular constituents of the atmosphere.

With a very high resolution spectrometer, it would be possible to observe these individual lines and to deduce wavelength transmission coefficients with a resolution commensurate with the observed line structure. For many applications, such detail is unnecessarily complex, and observations may be made under low resolution. In this case, the spectrometer "sees" many lines simultaneously and resolves only the coarse band structure. For this situation, band model approximations have been devised which predict the average transmission over a number of lines. From the low-resolution observations, transmission coefficients may be obtained which may be used with the appropriate band model approximation to calculate the transmission.

Gates (Ref. 2) has presented atmospheric transmission data for the near infrared, and Gates and Harrop (Ref. 3) presented data for wavelengths out to 12.5 micrometers. Although our observations extend from 12.5 to beyond 21.0 micrometers, only those in the region from 16.75 to 20.95 micrometers were deemed suitable for presentation. Since this region does not contain a good window, and since, in any case, the determination of the continuum attenuation is somewhat arbitrary, we have combined the continuum attenuation with the selective attenuation and have analyzed the data for selective transmission only.

The authors gratefully acknowledge the contributions of Mr. W. F. Fountain of the Space Sciences Laboratory, Marshall Space Flight Center, who computed the relative extraterrestrial solar spectral response shown in Figure 4, and who read all of the signal values from the scans.

THE OBSERVATIONS

The solar spectrum observations were made on two clear, cool days, March 21 and 23, 1970, from Bigelow Mountain, Arizona. This site is located in the Catalina Mountains, northeast of Tucson, at an altitude of 2,570 meters. Because of the climate and altitude, astronomical sources observed from this site are attenuated by relatively small amounts of water vapor.

A Perkin-Elmer Model SG-4 Telescope-Scanning Spectrometer was used to make the observations. This instrument, shown schematically in Figure 1, consists of Dall-Kirkham fore-optics feeding an Ebert spectrometer. After passing through the exit slit, the radiation passes through a spectral isolation filter and is focused onto the detector by means of an ellipsoidal mirror. The system has an effective f-number of 2.5, a spectrometer focal length of approximately 18 centimeters, and a grating ruled with 40 lines/millimeter. Entrance and exit slits were set at a width of 2 millimeters and the entrance slit was limited to a length of 2 millimeters so as to admit only the central portion of the 3-millimeter diameter solar image. The spectral slit width varied over the scans from 0.245 micrometer at 12.5 micrometers to 0.215 micrometer at 21.0 micrometers. All scanning was done in the first order, and the filter served to block higher orders and scattered light. A thermistor detector was used.

Forty-seven solar spectral scans were made during the two days of observation over a range of values of air mass and precipitable water. These scans were alternated with scans of the sky background. Of the 47 scans, the 38 selected for analysis were averaged, mostly in pairs, to provide two sets of 18 scans each; one set for various values of the air mass and the other set for various values of the precipitable water in the path. This was done to reduce some of the noise appearing in

NOTES:

M_1 – ELLIPSOIDAL MIRROR
M_2 – SPHERICAL MIRROR
S_1 – ENTRANCE SLIT
M_3 – PARABOLOIDAL MIRROR
G – GRATING
S_2 – EXIT SLIT
M_5 – FLAT MIRROR
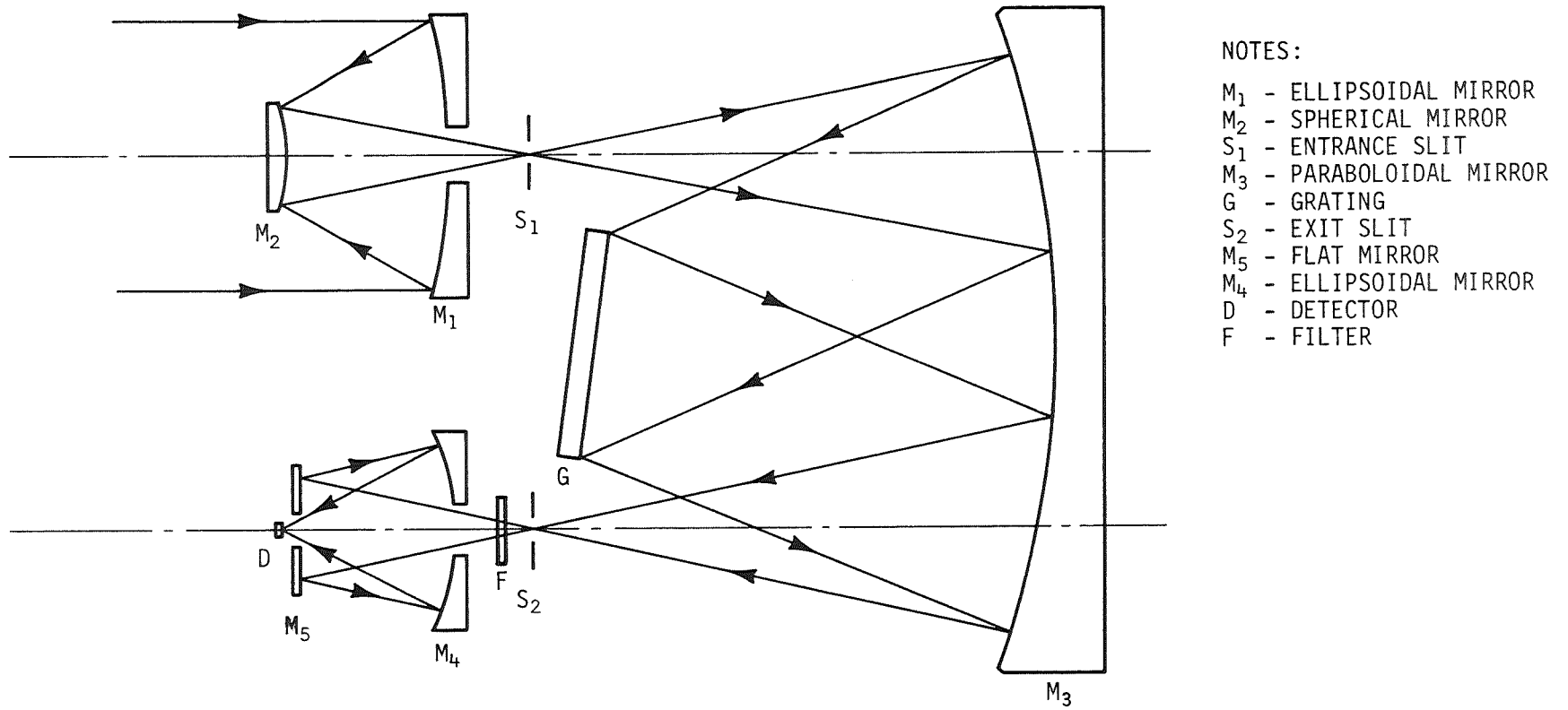M_4 – ELLIPSOIDAL MIRROR
D – DETECTOR
F – FILTER

FIGURE 1.   OPTICAL SCHEMATIC OF THE PERKIN-ELMER MODEL SG-4 TELESCOPE-SPECTROMETER

the original scans. The wavelength scale was placed by a comparison of observed bands in our spectra with those shown in the spectra of Farmer and Key (Ref. 4) and is probably accurate to ±0.05 micrometer. Absolute calibration scans of laboratory black body sources at 1,273°K and 300°K were also recorded.

It should be recalled that air mass is defined as the ratio of the slant path length through the atmosphere to the vertical path length for an observer at sea level. For a location above sea level, this value must be mutliplied by the ratio of the pressure to that at sea level. Air mass values for the scans were obtained by calculating the secants of the solar zenith angles, adding corrections for curvature of the atmosphere and for refraction, and finally multiplying by the ratio of pressures.

The values of precipitable water in the path were obtained by observing the selective absorption of a water band at 1.13 micrometers with a separate calibrated instrument. The air mass values were used to obtain vertical-column precipitable water values, which are plotted in Figure 2. Since the values of precipitable water were observed only intermittently, values for the separate scans were read from the graphs and converted to slant path values by using the air mass values.
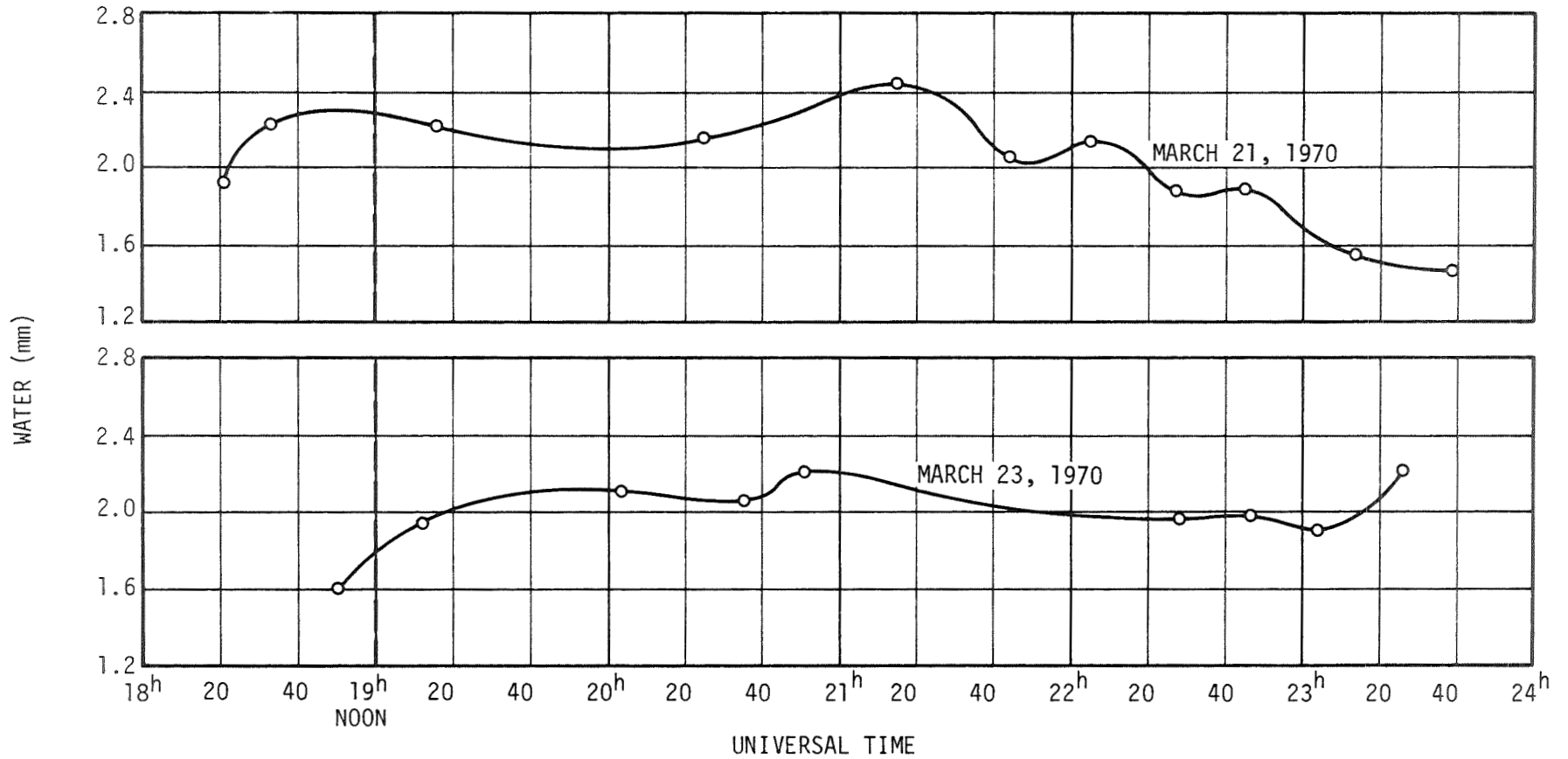
FIGURE 2.   PRECIPITABLE WATER IN A VERTICAL COLUMN OVER BIGELOW MOUNTAIN, ARIZONA

BAND MODEL APPROXIMATIONS

A close examination of almost any portion of the infrared solar spectrum, recorded from the ground under high resolution, reveals a complicated array of absorption lines. Furthermore, such an examination reveals that the precise mathematical description of the detailed wavelength variation of the absorption coefficient would be highly complex. However, such detail is not necessary, since band models have been devised which represent the absorption of an infrared band with reasonable accuracy. Two band models of interest here are the random (or statistical) band model and the regular (or Elsasser) band model. In many portions of the infrared spectrum, these models satisfactorily describe absorption by water and carbon dioxide, the two most important atmospheric absorbers. In the strong and weak line limits, approximations to these band models may be derived which may be easily fitted to the observational data and which may be used to calculate the transmission (or absorption) to sufficient accuracy for many applications. A number of band model approximations and arguments should be considered, since no single approximation would be expected to fit best throughout the spectrum.

The random (or statistical) band model has been derived by Goody with the assumption that the spectral lines have random spacing. A function describing the distribution of intensities of the lines must be specified, but this may be any function whatsoever. Perhaps the most commonly used distribution function is the exponential distribution (Ref. 5). This function states that the probability of finding a spectral line with an intensity between S and S + dS is

$$P(S) \, dS \; = \; \frac{dS}{S_0} \, \exp \, (-S/S_0) \qquad\qquad (1)$$

where S_0 is a parametric mean line intensity. For this distribution, the average transmission over many lines, as given by the random band model, is (Ref. 6)

$$\tau = \exp\left[\frac{-\beta X_0}{(1 + 2X_0)^{\frac{1}{2}}}\right] \quad , \tag{2}$$

where

$$\beta = \frac{2\pi\alpha}{d} \tag{3}$$

and

$$X_0 = \frac{S_0 \, u}{2\pi\alpha} \quad . \tag{4}$$

The half-width α is assumed to be the same for all the lines, and d is the mean spacing of the lines. The quantity u is the mass of absorbing gas per unit area in the path. This model has been used satisfactorily to represent absorption from the disordered array of lines characterizing water bands. The two approximations of this model of interest occur when the lines are strong and when they are weak. For the strong-line approximation (X_0 large), Equation 2 reduces to

$$\tau \approx \exp\left(-\frac{\beta}{\sqrt{2}} X_0^{\frac{1}{2}}\right) \quad . \tag{5}$$

For the weak-line approximation (X_0 small), Equation 2 reduces to

$$\tau \approx \exp\left(-\beta X_0\right) \quad . \tag{6}$$

Elsasser (Ref. 7) has derived a model to explain the absorption on the assumption of uniform, evenly spaced lines. This model satisfactorily explains absorption by the regularly spaced lines of many carbon dioxide bands. The exact expression for the transmission of a regular (Elsasser) band is (Ref. 8)

$$\tau = \frac{1}{2\pi} \int_{-\pi}^{\pi} \exp\left(\frac{-\beta X \sinh \beta}{\cosh \beta - \cos Z}\right) dZ \quad , \tag{7}$$

where β is defined above and

$$X = \frac{Su}{2\pi \alpha} \quad . \tag{8}$$

When the lines are strong, Equation 7 reduces to (Ref. 9)

$$\tau \approx 1 - \text{erf}\left(\frac{1}{2} \beta^2 X^{\frac{1}{2}}\right) \quad , \tag{9}$$

which may be approximated by (Ref. 3)

$$\tau \approx 1 - \left(\frac{2\beta X}{\pi}\right)^{\frac{1}{2}} \quad . \tag{10}$$

When the lines are weak, Equation 7 reduces to (Ref. 9)

$$\tau = \exp(-\beta X) \quad . \tag{11}$$

Note that the weak-regular band model approximation is identical to the weak-random band model approximation for $S = S_0$. Note, also, that in all of the band models, the quantities α, d, S_0, S, and, therefore, β, X_0, and X vary with wavelength throughout the spectrum.

When attempting to represent slant path atmospheric transmission by the band model approximations in regions of heavy water absorption, it is convenient to use as the argument the precipitable water in the path, w (expressed as a thickness). Other absorbers are relatively well-mixed in the atmosphere, and use of the air mass, m, is satisfactory.

For use in calculating slant path atmospheric transmission, the above band model approximations may be expressed as follows:

$$\tau = \frac{V}{V_0} \approx \exp\left(-C_1 m^{\frac{1}{2}}\right), \quad \text{strong-random,} \tag{12}$$
$$\text{air mass;}$$

$$\tau = \frac{V}{V_0} \approx \exp\left(-C_2 m\right), \quad \text{weak, air mass;} \tag{13}$$

$$\tau = \frac{V}{V_0} \approx 1 - C_3\, m^{\frac{1}{2}}, \quad \text{strong-regular,} \tag{14}$$
$$\text{air mass;}$$

$$\tau = \frac{V}{V_0} \approx \exp\left(-C_4 w^{\frac{1}{2}}\right), \quad \text{strong-random,} \tag{15}$$
$$\text{water}$$

$$\tau = \frac{V}{V_0} \approx \exp\left(-C_5 w\right), \quad \text{weak, water;} \tag{16}$$

and

$$\tau = \frac{V}{V_0} \approx 1 - C_6\, w^{\frac{1}{2}}, \quad \text{strong-regular,} \tag{17}$$
$$\text{water .}$$

The definition of transmission in terms of the terrestrial, V, and extra atmosphere, V_0, signals has been included. Note that a plot of $\ln \tau$ as a function of $m^{\frac{1}{2}}$ (or $w^{\frac{1}{2}}$) will yield a line of slope C_1 (or C_4) for the strong-random approximation, a plot of $\ln \tau$ as a function of m (or w) versus $m^{\frac{1}{2}}$ (or $w^{\frac{1}{2}}$) will yield a line of slope C_2 (or C_5) for the weak approximation, and a plot of τ will yield a line of slope C_3 (or C_6) for the strong-regular approximation. Note further that even if only the terrestrial signal values, V, are known, the coefficients may still be determined by using V instead of τ in the plots, with the coefficient C_3 (or C_6) equal to the slope/intercept.

DATA REDUCTION

The first step in data reduction was to divide the two sets of spectral scans into wavelength intervals. No effort was made to make them of uniform width, and they varied from 0.1 to 0.2 micrometer in width. They were selected so that intervals were centered at the tops of peaks and in the bottoms of bands. They were also chosen so that the spectral curves had negligible variation within the intervals. The signal values, corrected for sky background, were read in each interval in each scan and punched onto IBM data cards. Although 48 intervals from 12.5 to 20.95 micrometers were originally chosen and measured, only the last 26 from 16.75 to 20.95 micrometers were finally deemed suitable for presentation.

The next step was to determine the extraterrestrial signal envelope. This is the scan that the instrument would produce if it were directed at the Sun from outside the atmosphere. This envelope was determined so that the fit of the various band model approximations, to be numerically calculated later, could be placed on a consistent, meaningful scale. The signal values for the three peaks at 13.50, 17.75, and 18.60 micrometers were plotted as $\ln$ (signal) as a function of air mass. These plots are shown in Figure 3, along with the least square lines. The antilogs of the zero air mass intercepts of these lines should be extraterrestrial signal values of the instrument at these wavelengths.

The signal difference indicated by the telescope-spectrometer to black body sources at two temperatures may be represented by

$$V_1 - V_2 = \left| B(\lambda_1, T_1) - B(\lambda_1, T_2) \right| \frac{A_T A_S}{F^2} \tau_S(\lambda) R_D(\lambda) \Delta\lambda(\lambda). \tag{18}$$

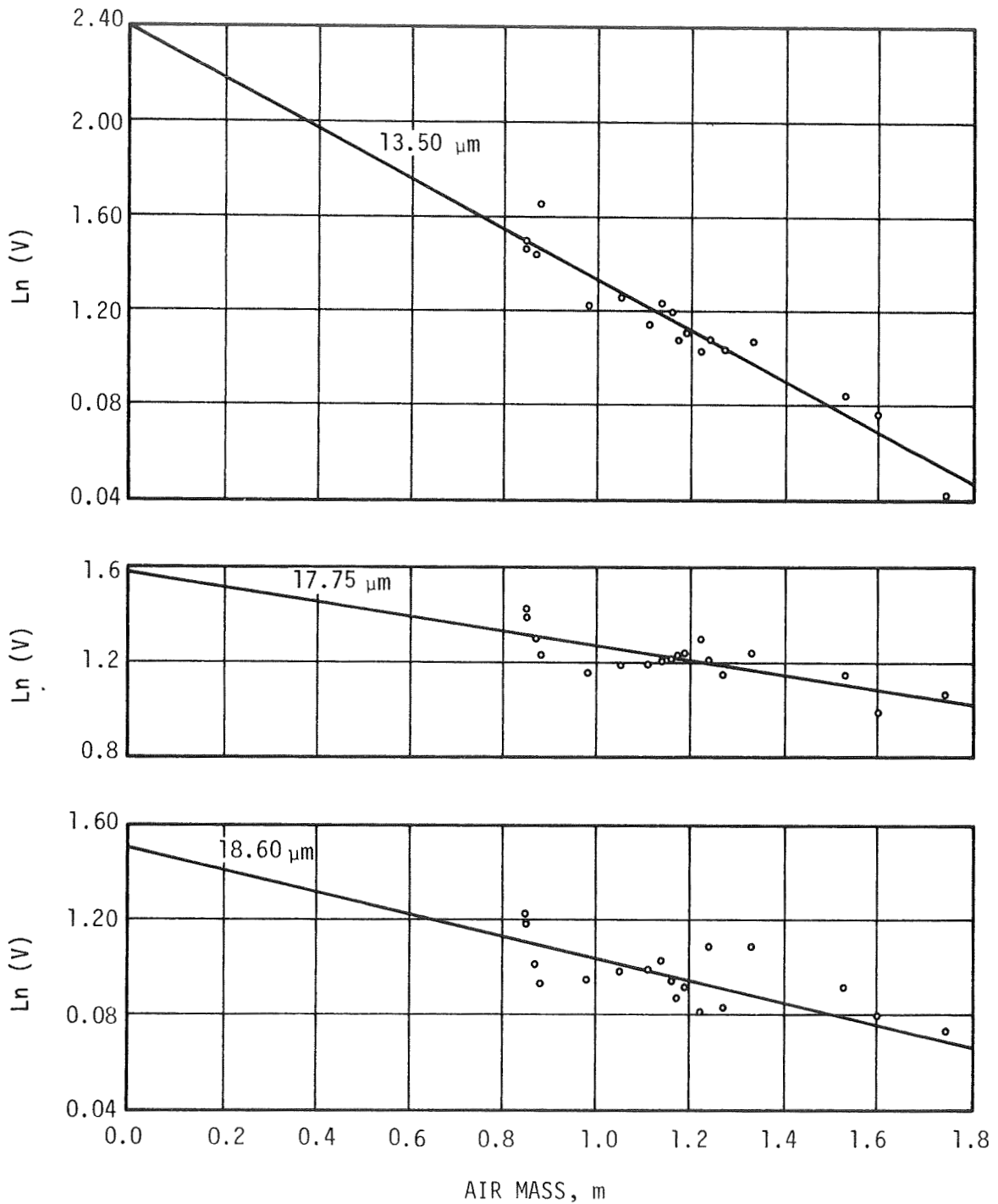FIGURE 3. Ln (SIGNAL) AS A FUNCTION OF AIR MASS AT
THREE WAVELENGTHS

Here

$B(\lambda, T)$ – Planck function expressed as a radiance

A_T – collecting area of the telescope

A_S – area of the entrance slit

$R_D(\lambda)$ – detector responsivity

$\Delta\lambda(\lambda)$ – spectral slit width

$\tau_S(\lambda)$ – overall reflectance of the mirrors, grating efficiency, and filter transmission.

Differences are used so that any background is cancelled. The determination of the product $\tau_S(\lambda)\, R_D(\lambda)\, \Delta\lambda(\lambda)$ as a function of the wavelength would constitute an absolute calibration of the system. Previous data indicate that the solar spectral energy distribution in the far infrared may be represented to reasonable accuracy by the Planck function for 5,000°K (Refs. 3 and 4). Then, the extraterrestrial solar signal is

$$V_\odot = B(\lambda, T_\odot) \frac{A_T A_S}{F_\odot^2} \tau_S(\lambda)\, R_D(\lambda)\, \Delta\lambda(\lambda) \ . \tag{19}$$

The focal length $F_\odot$ is the infinity focus and is slightly smaller than the focal length F for the black body sources. Combining Equations 18 and 19 yields

$$V_\odot = \left(\frac{F}{F_\odot}\right)^2 \frac{V_1 - V_2}{B(\lambda_1, T_1) - B(\lambda_1, T_2)} B(\lambda_1, T_\odot) \ . \tag{20}$$

Black body scans taken for 1,273°K and 300°K were used with Equation 20 to calculate the shape of the extraterrestrial signal envelope. No effort was made at first to evaluate the scale factor of the envelope indicated by Equation 20. This envelope, and the extraterrestrial signal values indicated by extrapolation of the plots of Figure 3, were each

13

plotted as a function of wavelength on logarithmic scales. The envelope could then be fitted to the signal values simply by sliding the curve over the points. The best fitting position then provided the desired envelope. This envelope and the points used are shown in Figure 4. A typical instrumental scan is also shown by the solid curve. This graph and the assumption of black body solar spectral radiance were used to obtain Figure 5.

This extraterrestrial envelope was checked in the following three ways. Equation 20 was used to find the extraterrestrial curve absolutely. Extrapolations in other wavelength intervals with other band model approximations were tried. Also, data of Taylor and Yates (Ref. 10) and of Farmer and Key (Ref. 4) indicated scale factors for the extra-terrestrial curve. All of these checks revealed that the height of the true extraterrestrial signal envelope is somewhat uncertain. However, all considerations indicate that the extraterrestrial curve shown in Figure 4, which was the one adopted, is the most accurate one which may be obtained from these data.

The signal values for each of the intervals were read from the extraterrestrial curve, and these were punched onto IBM data cards. The remaining data reduction, except for the plotting of graphs, was done by computer. The computer was programmed first to find trans-missions by dividing all of the signal values by the appropriate values read from the extraterrestrial envelope.

Next, the computer found slopes and zero argument intercepts for least square lines fitted to plots of the transmission in all of the intervals, plotted in six ways: $\ln \tau$ as a function of $m^{\frac{1}{2}}$, $\ln \tau$ as a function of m, τ as a function of $m^{\frac{1}{2}}$, $\ln \tau$ as a function of $w^{\frac{1}{2}}$, $\ln \tau$ as a function of w, and τ as a function of $w^{\frac{1}{2}}$. For the strong-regular plots, the computer found the values of the slope divided by the intercept.
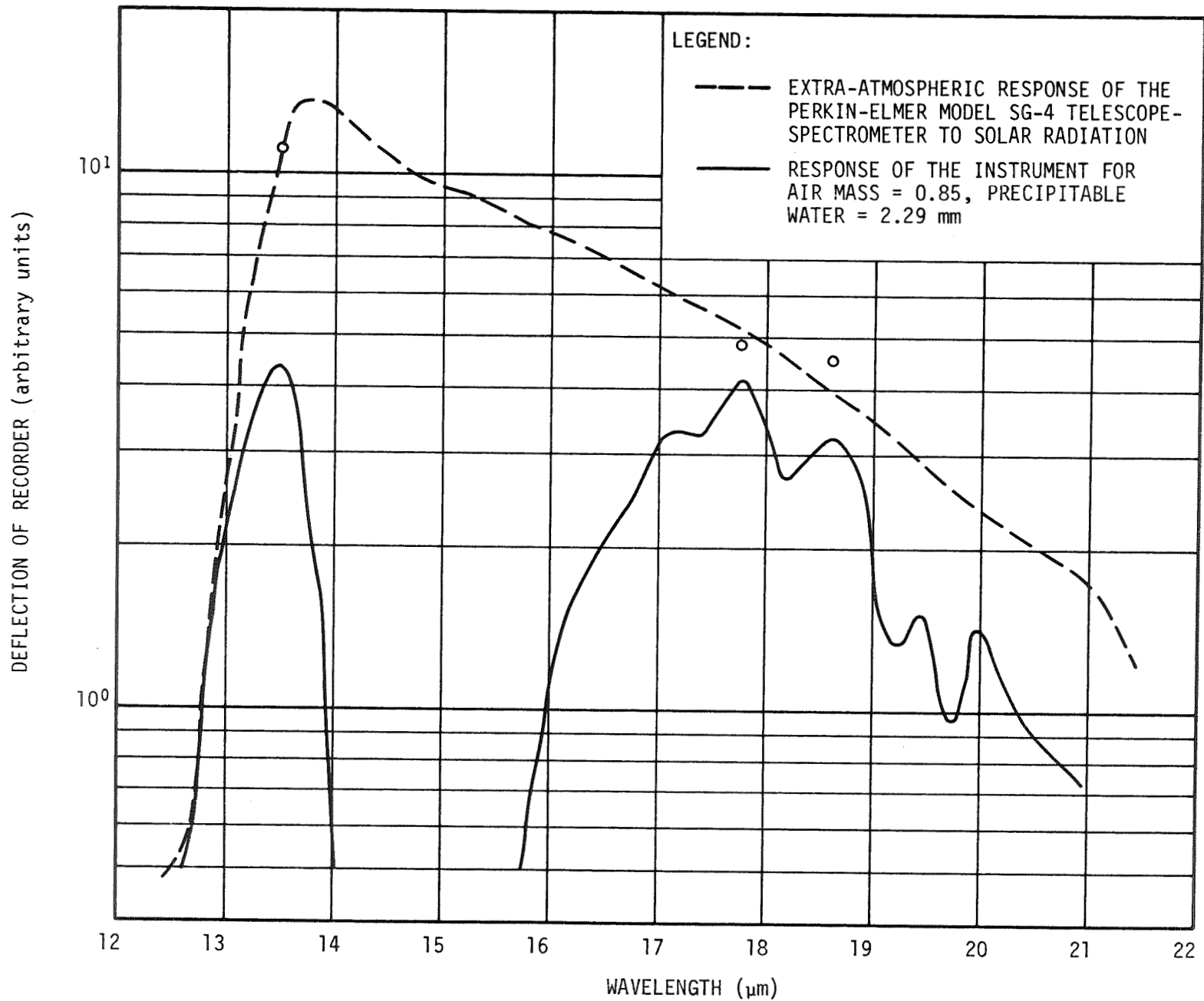
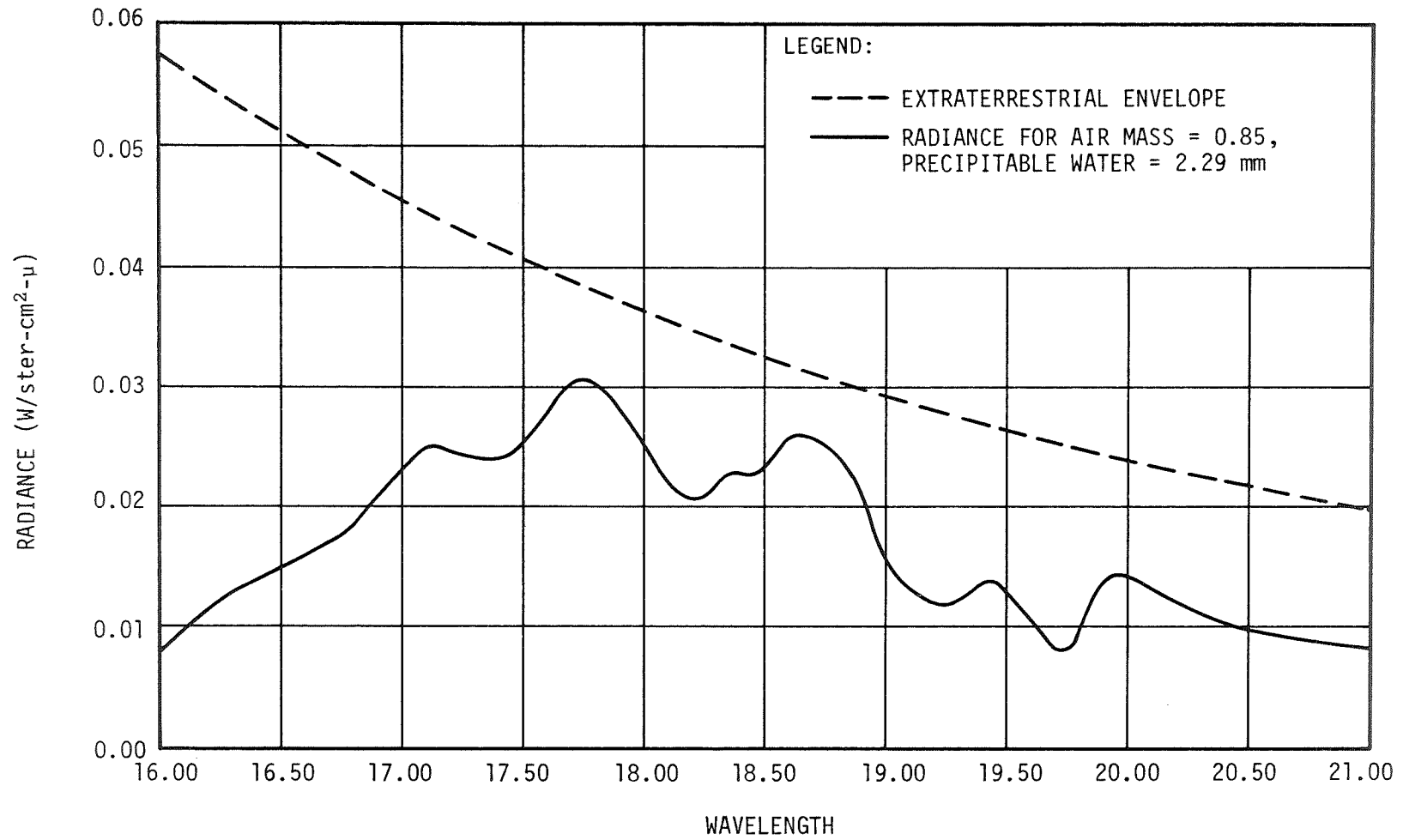FIGURE 4. TERRESTRIAL AND EXTRATERRESTRIAL RESPONSE OF THE TELESCOPE-SPECTROMETER TO SOLAR RADIATION

FIGURE 5. LOW RESOLUTION SOLAR SPECTRAL RADIANCE FROM 16 TO 21 MICROMETERS

The attenuation coefficients C_1, C_2, C_4, C_5 are just the slopes of the corresponding plots, and the coefficients C_3, C_6 are the values of the slope/intercept. Values of the sum of squares of the deviations of the observed transmissions from the least squares lines were also printed out. These provide an evaluation of the fit of the various band model approximations and arguments.

An alternative procedure would be to require that the lines fitted to the attenuation plots pass through unity transmission for the argument value of zero. If the extraterrestrial envelope were well known, this procedure would yield improved values of the attenuation coefficients and better distinction between the fit of the various band model approximations. However, because of the aforementioned uncertainty in this envelope, this method could force needless systematic errors into the attenuation coefficients.

RESULTS

The attenuation coefficients for air mass argument and for precipitable water argument are presented in Tables 1 and 2. Values of the sum of squares of the deviations of the observed transmissions from the least square line fits are also presented. It should be recalled that 18 points were used for these calculations. At each wavelength, the smallest value of this quantity indicates the best fitting band model approximation and argument according to our data. The attenuation coefficient for the strong-random approximation, precipitable water argument is plotted in Figure 6. As expected, this curve is very roughly a mirror image of the terrestrial solar spectral radiance shown in Figure 5.

The deviation values are plotted in Figure 7. The sets of air mass and precipitable water curves illustrate only weakly the differences in fit between the various band model approximations; they are dominated by wavelength variations in the random scatter of the observed points. This behavior is caused not only by random scatter, but also by the limited range in air mass (or precipitable water) of the observations and by the least square line fits. These least square line fits to the attenuation plots will approximate the average tangents to the attenuation curves over the ranges observed. The random scatter of the observed points about the attenuation curves should be the same for all band model approximations. Because of the limited range in argument of the observations, the random scatter about the average tangents, and, therefore, about the least square line fits, will approximately equal the random scatter about the curves. Therefore, the sum of squares of deviations indicated in Figure 7 will be approximately identical for all band model approximations with each argument in each wavelength interval except for small variations resulting from differences in the band model approximations themselves. Better data are needed.

TABLE 1. TRANSMISSION COEFFICIENTS FOR AIR MASS ARGUMENT

Wavelength (micrometer)	C_1 (Air Mass)$^{-\frac{1}{2}}$	$\sum(\Delta t)^2, C_1$	C_2 (Air Mass)$^{-1}$	$\sum(\Delta t)^2, C_2$	C_3 (Air Mass)$^{-\frac{1}{2}}$	$\sum(\Delta t)^2, C_3$	Dominant Absorber
16.75	2.55×10^0	1.07×10^{-2}	1.16×10^0	1.01×10^{-2}	6.58×10^{-1}	9.68×10^{-3}	CO_2
16.85	2.27	1.18	1.04	1.12	6.40	1.10×10^{-2}	CO_2
17.00	1.88	8.25×10^{-3}	8.52×10^{-1}	8.72×10^{-3}	6.10	9.79×10^{-3}	CO_2
17.20	1.68	3.89×10^{-2}	7.67	3.80×10^{-2}	5.81	3.76×10^{-2}	H_2O
17.40	1.17	2.56	5.35	2.53	5.04	2.50	H_2O
17.60	1.06	6.10	4.84	6.01	4.88	5.99	H_2O
17.75	7.20×10^{-1}	3.97	3.26	4.03	4.04	4.00	H_2O
17.90	6.33	2.64	2.87	2.67	3.72	2.65	H_2O
18.00	8.11	4.12	3.71	4.03	4.24	4.02	H_2O
18.10	8.99	5.58	4.16	5.43	4.36	5.39	H_2O
18.20	9.61	3.80	4.44	3.67	4.54	3.63	H_2O
18.35	8.83	6.31	4.01	6.34	4.45	6.30	H_2O
18.60	9.57	7.65	4.35	7.68	4.63	7.64	H_2O
18.80	9.18	8.12	4.16	8.15	4.56	8.11	H_2O
19.00	1.12×10^0	7.87	5.11	7.82	4.83	7.74	H_2O
19.25	1.75	5.96	7.86	6.06	5.85	6.08	H_2O
19.45	1.45	5.49	6.44	5.80	5.66	5.86	H_2O
19.60	2.21	4.76	1.01×10^0	4.79	6.27	4.78	H_2O
19.80	1.77	6.26	8.17×10^{-1}	6.09	5.72	5.81	H_2O
19.95	1.40	5.49	6.45	5.30	5.38	5.14	H_2O
20.15	1.02	5.23	4.72	5.07	4.65	5.01	H_2O
20.40	1.13	7.64	5.17	7.62	4.72	7.50	H_2O
20.55	1.50	8.58	6.82	8.57	5.34	8.42	H_2O
20.65	1.82	8.07	8.31	7.88	5.74	7.58	H_2O
20.80	1.56	1.42×10^{-1}	7.23	1.39×10^{-1}	5.11	1.30×10^{-1}	H_2O
20.95	1.16	7.96×10^{-2}	5.29	7.93×10^{-2}	4.37	7.62×10^{-2}	H_2O

TABLE 2.   TRANSMISSION COEFFICIENTS FOR PRECIPITABLE WATER ARGUMENT

Wavelength (micrometer)	C_4 (mm)$^{-\frac{1}{2}}$	$\sum(\Delta\tau)^2, C_4$	C_5 (mm)$^{-1}$	$\sum(\Delta\tau)^2, C_5$	C_6 (mm)$^{-\frac{1}{2}}$	$\sum(\Delta\tau)^2, C_6$	Dominant Absorber
16.75	1.44×10^0	3.64×10^{-2}	3.62×10^{-1}	4.06×10^{-2}	3.89×10^{-1}	4.32×10^{-2}	CO_2
16.85	1.38	2.90	3.54	3.13	3.82	3.45	CO_2
17.00	1.12	4.41	2.85	4.88	3.63	5.16	CO_2
17.20	1.04	3.95	2.70	4.18	3.51	4.35	H_2O
17.40	8.24×10^{-1}	2.52	2.14	2.65	3.22	2.70	H_2O
17.60	8.89	3.00	2.31	3.26	3.32	3.39	H_2O
17.75	5.50	5.23	1.40	5.63	2.75	5.56	H_2O
17.90	3.21	7.39	7.94×10^{-2}	7.67	2.06	7.51	H_2O
18.00	3.44	4.60	8.55	4.83	2.14	4.71	H_2O
18.10	5.87	5.65	1.50×10^{-1}	5.86	2.78	5.84	H_2O
18.20	5.56	6.31	1.41	6.54	2.73	6.49	H_2O
18.35	5.73	6.54	1.46	6.83	2.78	6.79	H_2O
18.60	6.73	7.06	1.73	7.37	2.98	7.38	H_2O
18.80	5.52	1.06×10^{-1}	1.41	1.09×10^{-1}	2.75	1.08×10^{-1}	H_2O
19.00	9.72	1.70	2.48	1.76	3.52	1.75	H_2O
19.25	1.08×10^0	9.26×10^{-2}	2.78	9.41×10^{-2}	3.53	9.30×10^{-2}	H_2O
19.45	1.03	7.52	2.64	7.93	3.58	7.97	H_2O
19.60	2.22	6.54	5.88	6.02	4.05	5.59	H_2O
19.80	1.94	7.02	5.13	6.69	4.00	6.39	H_2O
19.95	1.23	7.13	3.20	7.23	3.67	7.37	H_2O
20.15	7.92×10^{-1}	7.23	2.07	7.20	3.13	7.18	H_2O
20.40	9.22	7.60	2.42	7.44	3.23	7.37	H_2O
20.55	9.58	5.97	2.47	6.07	3.20	6.13	H_2O
20.65	8.80	7.69	2.26	7.89	3.00	7.88	H_2O
20.80	1.11×10^0	6.37	2.92	6.09	3.24	5.67	H_2O
20.95	1.31	1.07×10^{-1}	3.46	1.04×10^{-1}	3.55	9.88	H_2O
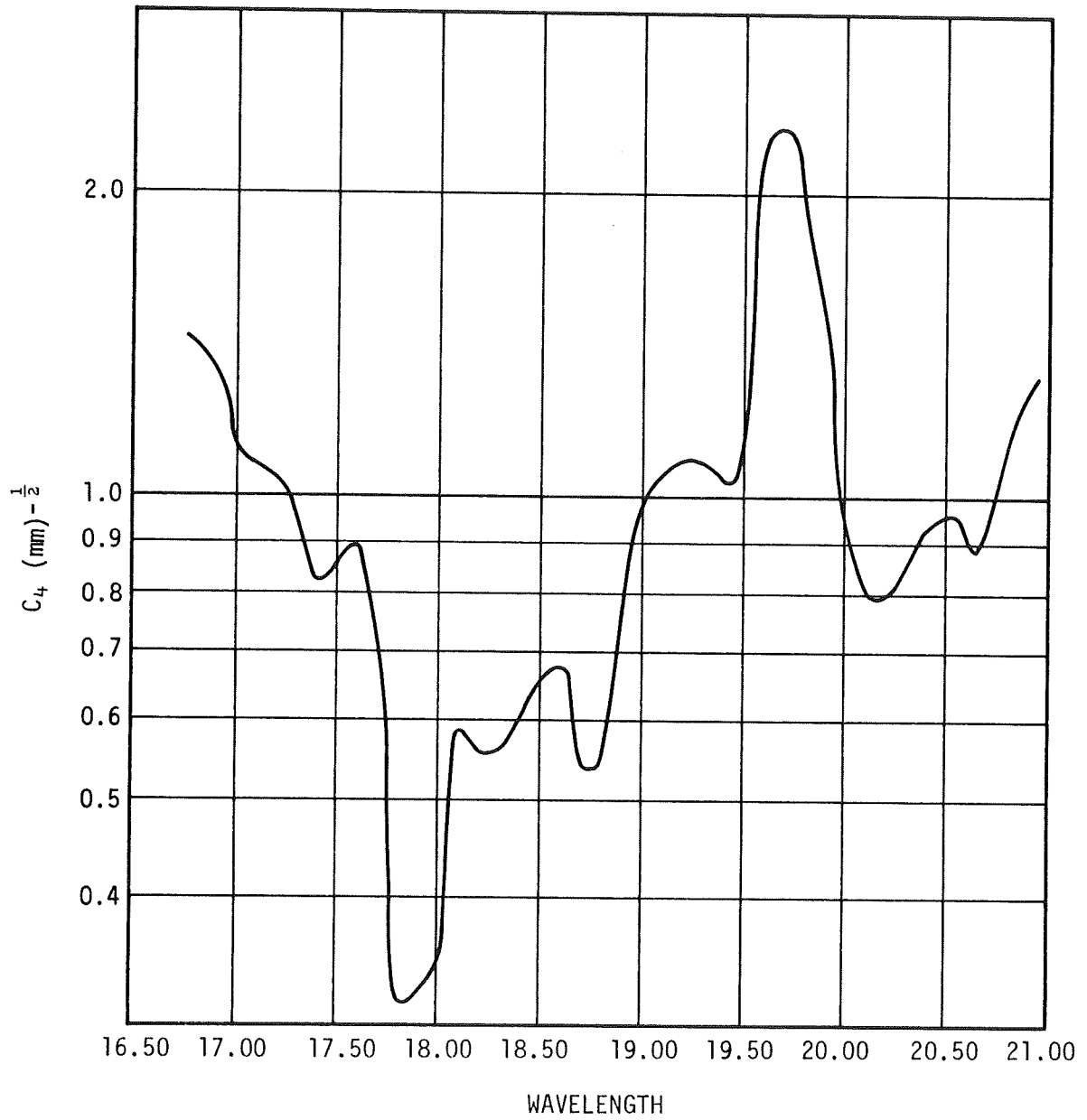
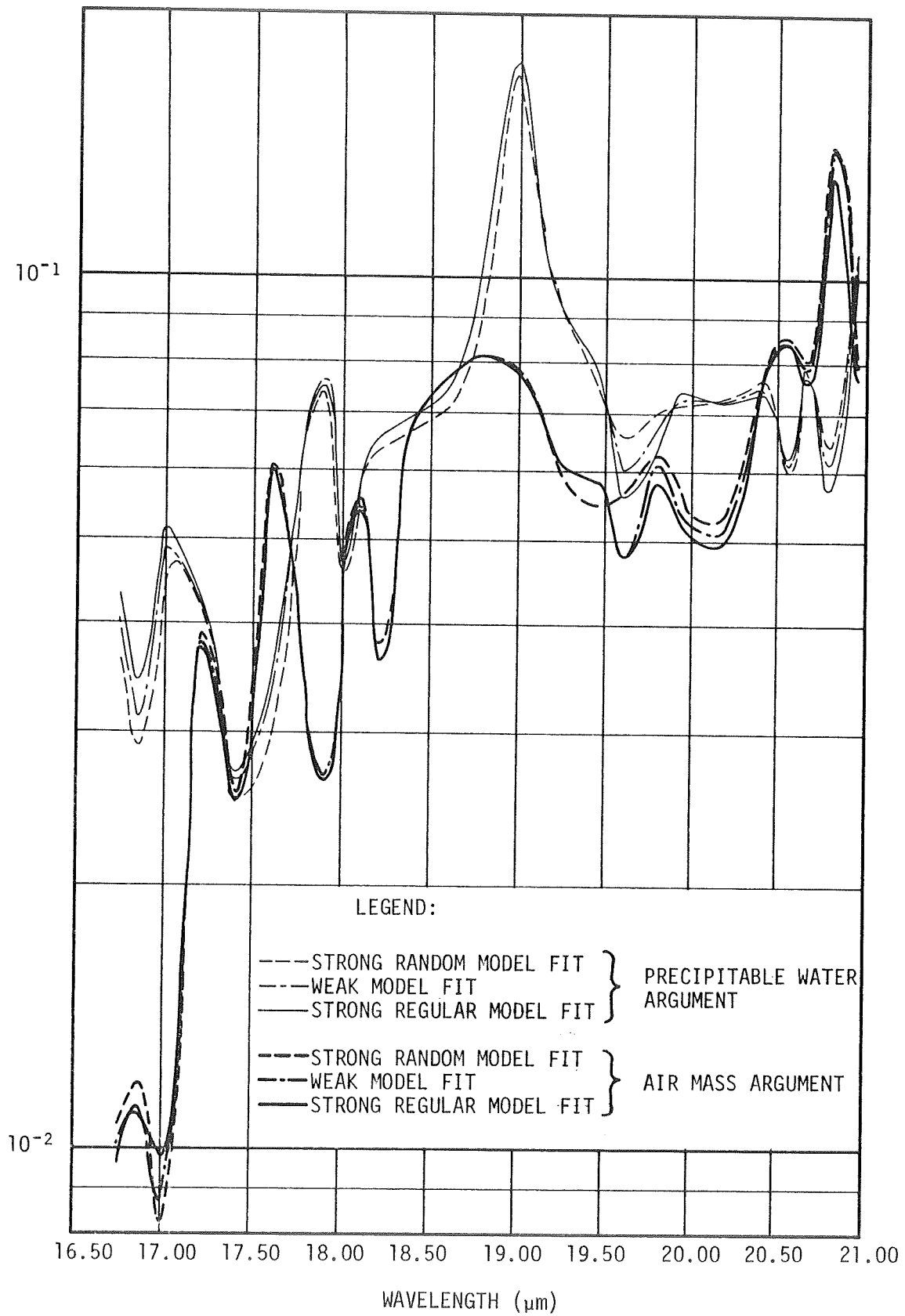FIGURE 6. WAVELENGTH VARIATION OF THE ATTENUATION COEFFICIENT C_4

FIGURE 7. THE QUALITY OF FIT OF THE VARIOUS BAND MODEL APPROXIMATIONS

Note that for wavelengths shorter than 17.2 micrometers, the curves of Figure 7 indicate that the use of air mass as argument provides a distinctly better fit to the data. This region lies in the wing of the strong 15-micrometer band of carbon dioxide, a gas which is relatively well-mixed in the atmosphere.

REFERENCES

1. Raine, W. L. and S. M. Landrum, Jr., "Use of a Direct-Imaging Filtered Radiometer for the Measurement of Lunar Brightness Temperatures", Teledyne Brown Engineering, Summary Report RL-SSL-437, February 1969

2. Gates, D. M., "Near Infrared Atmospheric Transmission to Solar Radiation", Journal of the Optical Society of America, 50, No. 12, p. 1299, December 1950

3. Gates, D. M. and W. J. Harrop, "Infrared Transmission of the Atmosphere to Solar Radiation", Applied Optics, 2, No. 9, p. 887, September 1963

4. Farmer, C. G. and P. J. Key, "A Study of the Solar Spectrum From 7μ to 400μ", Applied Optics, 4, No. 9, p. 1051, September 1965

5. Handbook of Military Infrared Technology, W. L. Wolfe, Editor, (Washington: Naval Research Laboraotry) Chapter 6, 1965

6. Plass, G. N., "Models for Spectral Band Absorption", Journal of the Optical Society of America, 48, No. 10, p. 690, October 1958

7. Elsasser, W. M., "Heat Transfer by Infrared Radiation in the Atmospheric", Harvard Meteorological Studies, No. 6, Harvard University Press, Cambridge, Massachusetts, 1942

8. Elsasser, W. M., Physical Review, 54, p. 126, 1938

9. Plass, G. N., "Useful Representations for Measurements of Spectral Band Absorption", Journal of the Optical Society of America, 50, No. 9, p. 868, 1960

10. Yates, H. W., and J. H. Taylor, "Infrared Transmission of the Atmosphere", NRL Report 5453, U. S. Naval Research Laboratory, Washington, D. C., ASTIA AD 240188, 1960